REVIEW OF AERONAUTICAL FATIGUE INVESTIGATIONS IN JAPAN DURING THE PERIOD JUNE 2003 TO JUNE 2005

Edited by
Akira Kobayashi
Science University of Tokyo

and

Hiroyuki Terada
Japan Aerospace Technology Foundation

For Presentation at the 29th Conference of
The International Committee on Aeronautical Fatigue

Hamburg, Germany, June 7, 2005

12.1 INTRODUCTION

A. Kobayashi, National Delegate

The present national review reports aeronautical fatigue activities in Japan during 2003 to 2005. The review is due to contributions by Aeronautical Fatigue Research Committee members of Japan Society for Aeronautical and Space Sciences, especially to the key members affiliated with the following:

Japan Aerospace Technology Foundation
Japan Aerospace Exploration Agency
Japan Defense Agency
Aircraft and Railway Accidents Investigation Commission
Japan Aircraft Development Corporation
Mitsubishi Heavy Industries
Kawasaki Heavy Industries
Fuji Heavy Industries
Toyota Motor Corporation
Tokyo Metropolitan Institute of Technology
Shonan Institute of Technology
The University of Tokyo

The above-mentioned members are greatly appreciated for their concentrated endeavor to achieve such a fruitful review. Mr. Tadao Kamiyama, former National Delegate of Japan, is acknowledged for his everlasting encouragement during the course of compilation of the present review.

12.2 FRACTURE MECHANICS

12.2.1 Stress Intensity Factor Analysis and Fatigue Behavior of a Crack in the Residual Stress Field of Welding

Hiroyuki Terada, Japan Aerospace Technology, Tokyo Japan, E-mail hterada@dance.ocn.ne.jp

This paper deals with the behavior of a crack in the residual stress field induced by butt weld in a wide plate. It is known that the distribution pattern of residual stress is similar regardless of welding process, though the size and the magnitude of the residual stress depend largely on the welding process. Stress intensity factor and stress redistribution induced by the crack extension were calculated for a crack with arbitrary length and location. The stress redistributions caused by crack extension obtained by the present analysis showed good agreement with the experimental data. Fatigue crack propagation behavior in the residual stress field reported by Glinka was also examined from ΔK point of view. In this paper, the effect of residual stress on the fatigue crack propagation rate is considered to be the effect of varying mean stress. The concept of ΔKeff, where the effect of residual stress is accounted as the correction factor by the way of simple superposition, is shown to predict the crack growth rate with sufficient accuracy.

12.3 LIFE EVALUATION ANALYSIS

12.3.1 A Simplified Analysis on Bayesian Method of Structural Reliability under Scheduled Inspection

Seiichi Ito, Takao Okada, Japan Aerospace Exploration Agency (JAXA), and
Wang Bintuan, The First Aircraft Institute of AVIC-I, China

As a first step in reliability evaluation for an aging structure under periodic inspection, a simple method for grasping the outline of the reliability was proposed. The problem regarding integrity of an existing aging structure has come to occupy an important position in the structural reliability. In this report, the reliability analysis that can rationally estimate the characteristics of the uncertain parameters and the reliability of the aging structures is proposed with respect to the settlement of the inspection policy to maintain the structural integrity with the use of Markov chain and Bayesian theory. It is difficult to clearly define the degree of damage, such as corrosion fatigue defect, to a real structure. Therefore, damage size is not considered in this analysis to establish the conventional reliability analysis but the life of aging defect is expressed using a convolution integral which consists of probability distribution of initiation and propagation life. In the fatigue test results, it is shown that the fatigue life can be approximately modeled as a convolution distribution of the $F_I(t_i|\theta_i)$ and $F_P(t_p|\theta_p)$. The probability distribution aging degradation life t_c can be written as follows,

$$F_C(t_c \mid \theta_I, \theta_P) = \int_0^{t_c} F_P(t_c - t_i \mid \theta_p) f_I(t_i \mid \theta_I) dt_i$$

where t_i and t_p represent the vector of population parameters that define respectively the probability distribution of defect initiation and propagation life. In this report, the convolution distribution in above equation is applied to the reliability evaluation under the periodic structural inspection. With respect to drawing up of the inspection plan to suffice reliability of aging structures, formulation of probability event on periodic inspection is made using the above life assumption and the Markov transition probability matrix. The population parameter of the uncertain factors related to the aging defect and structural inspection is estimated by the results obtained from the inspection in accordance with the Bayesian method. To make certain of the effectiveness of this simplified method, we discuss, using numerical simulation, the way inspection schedules should be settled to maintain the integrity of aging structures. This method of analysis is not only concise but also convenient for practical use.

12.4 FATIGUE AND CORROSION IN METALLIC MATERIALS AND COMPONENTS

12.4.1 Behavior of Short Cracks in Corrosive Environments for 7075 Al Alloy

T. Okada, Japan Aerospace and Exploration Agency (JAXA)
e-mail: okada.takao@jaxa.jp

Degradation of fatigue life of airplane structure under corrosive environment has been widely known and it has recently been investigated that the selection of initial discontinuity size and corrosion scenarios has a large effect on the evaluation of fatigue life and decisions related to inspection intervals. Based on this circumstance and the progress in engineering technology, the research for the holistic life prediction has progressed and the evaluation of short crack growth behavior under corrosive environment is also necessary for this purpose.

For 7075-T6 extruded specimen cut from C-141 wing panel, pit growth testing under a couple of pre-corrosion and concomitant corrosion fatigue condition conducted by the University of Utah was presented in the previous conference. From the point of short crack growth, additional short crack growth tests under concomitant corrosion fatigue condition and scanning electron microscope (SEM) observation of the fracture surfaces for both specimens were conducted. The growth behavior of fatigue cracks nucleated at the corrosion pits or particles was monitored by CCD camera and SEM. To confirm the effect of microstructure, the fatigue cracks of which length was less than 100 μm were measured during the tests.

The fracture surface could be classified into two types shown in Figs. 12.1 and 12.2. For the first type, the origin of the fracture was a small corrosion pit that didn't show the delamination or exfoliation feature. Near the origin, the surface was plain without a few ridges of which direction would correspond to the crack growth direction. In the other case, the origin was a large corrosion pit which showed a delamination or exfoliation feature. The origin could be any location within the pit and there might be a couple of origins on the fracture surface. The feature of the fracture surface near the origin was different for each of specimens. The difference of boundary conditions at each origin would seem to affect the short crack growth behavior.

Fig. 12.3 shows the relationship between fatigue crack growth rate and crack length under different environmental intervals. Scatter of crack growth rate around its length of 100 μm is more than 10 and it seems to be an effect of microstructure. Additional data gives closer information.

12.4.2 Fatigue and Crack Propagation Properties of Friction Stir Welded Lap Joint and Panel

Hiroaki Satou and Toru Sakagawa, Mitsubishi Heavy Industries, LTD (MHI)

The friction stir welding (FSW) process expects tremendous potential of low cost, fastenerless jointing of high strength aluminum airframe structures, and also better welding quality of FSW joints than conventional fusion weld joints. In this study, for the application of FSW as joining method for the skin/stringers panel, mechanical properties of FSW lap joints and FSWed skin/stringers panels were studied.

Fatigue strength of several kinds of joints was evaluated comparing with those of riveted joints in order to clarify the welding joint characteristics. Fatigue strength of FSWed joints is normally superior to that of riveted joints, since there are no fastener holes which concentrate the stress. However, some joint configurations are found less characteristics to compare with that of rivet joints. We also evaluated the effect of surface treatment before welding. Some surface treatments improved fatigue strength of FSW joints because of prevention to the fretting at the joint.

Crack propagation properties of FSW joints were also evaluated. The residual stress at welding line is under tension related to the shrinkage of weld metal. There is compressive residual stress at outer area of FSW line. Therefore, crack propagation characteristics of FSW joint are much affected by residual stress. The existence of compressive residual stress prevents crack growth, while the existence of tension residual stress accelerates crack growth. We found the crack growth characteristics of FSW joint are dependent on the direction of applied stress and position of the initial crack.

Three and four stringers panels were fabricated respectively by applying the FSW and the rivet, then mechanical properties of these panels were evaluated. Panel buckling tests were conducted using three stringer panels. The bucking strength of FSWed panel is 8% stronger than that of riveted panel. FSW is continuous jointing between the skin and stringer similar to the integral panel. This continuous jointing increase the crippling strength of stringer, then buckling strength was improved.

Crack propagation properties were evaluated by using four stringer panels. There is compressive residual stress at skin area between stringers, and tension residual stress near stringer jointing area. At the first test saw cut was located at center between stringers. In this case compression residual stress applies at tip of crack, and crack growth rate of FSWed panel is much lower than that of riveted panel. This result can be explained by existence of residual stress. Other panel test is preparing, and the result will be presented at the symposium.

This study is supported by METI and NEDO.

12.4.3 Fatigue Properties of Friction Stir Welded Aluminum Alloy 6061

T. Nagayama, H. Takehisa and M. Shimanuki, Fuji Heavy Industries LTD, (FHI)

Friction Stir Welding (FSW) is an innovative solid phase welding process. This process has many advantages of elimination of voids, cracking, or distortion, and of reduction of manufacturing costs by leaving out filler metals, shielding gases and weld preparation which are necessary for fusion welding such as TIG. Furthermore, friction stir welds of aluminum alloys show better mechanical properties, especially fatigue properties, than those of fusion welds.

Based on this background, FHI developed the butt joint FSW process of thin 6061-O, -T6 sheets to apply it to UAV (unmanned aerial vehicle) structures as an assembly arrangement instead of TIG.

In the process of development, it was found that kissing bond, which is the defect of backside of welds, occurred when the plunge depth on a conventional FSW pin tool is not maintained in the proper location, has a negative effect on fatigue strength. Figure 12.4 shows the photograph of kissing bond and the results of fatigue tests. Consequently, the pin configuration and weld parameters to eliminate kissing bond were developed.

After establishing the FSW process including pin configuration, the fatigue tests of FSW welds were conducted again. The tests were performed on 1.27mm thick sheets of 6061-T6 and 0.81mm thick sheets of 6061-O. For UAV, these materials were used and fusion weld was applied. Parent sheets (6061-T6) and TIG welds (6061-T6 and O) were also tested to compare with the properties of FSW welds.

Figure 12.5 shows S-N data for parent sheets, TIG and FSW welds. Compared with the parent sheets, fatigue strength of FSW welds dropped by 15 - 20%. However, the strength of FSW is approximately 25% higher than that of TIG welds.

Figure 12.6 shows S-N data for TIG and FSW welds. Fatigue strength of FSW is higher than that of TIG all over the range.

As a consequence, it was found that FSW welds are superior to TIG welds in fatigue properties. Static tests were also conducted, and the superiority of FSW to TIG welds was also confirmed.

Accordingly, FSW process has been successfully applied to UAV fuselage and nacelle structure in lieu of TIG.

12.4.4 Element Fatigue Test of Wing Root Joint – Embraer 190 Aircraft

T. Taki, Kawasaki Heavy Industries, Ltd. (KHI), taki_toshimi@khi.co.jp

Objective of Test

Kawasaki Heavy Industries Ltd. (KHI) is developing the wing box structure of Embraer 190/195 as a risk sharing partner. One of the most critical areas of the wing box is the wing root joint. KHI and Embraer selected a shear joint design with spliced plates for the wing root joint. In order to obtain design data of the joint, KHI conducted joint element fatigue test.

Test Specimens

Two types of the test specimens were used. The first type (Type 1) is a straight specimen with two stringers as shown in Figure 12.7. Dihedral angle is added in another type (Type 2 specimen). The configuration of the both types of the test specimens simulates the critical area of the wing root joint. Wing skins and splice plates are made of the same aluminum alloy as the aircraft. Three rows of Hi-Lite fasteners are used in the joints. Sealing and surface treatment are also simulated in the test specimens.

Test Result

Strain surveys were conducted with the both types of the test specimens before fatigue test and stress distribution in the joint was obtained. This data was used to validate finite element analysis of the joint. Test setup of Type 2 test specimen is shown in Figure 12.8. A dummy rib to support the kick force produced by the dihedral angle was attached to a slide table.

Constant amplitude fatigue test of Type 1 specimens was performed with several stress levels and ratios, and S-N curves of the joint were developed. Flight-by-flight fatigue test of Type 2 specimens was performed and correlation between Type 1 and Type 2 was established.

Periodical ultrasonic inspection was performed in Type 2 test in order to determine detectable crack size in the same geometrical configuration as the actual aircraft. The ultrasonic inspection detected fatigue cracks around fastener holes in the test specimens. Using the data, we established the ultrasonic inspection procedure and determined the minimum detectable crack size for the joint.

12.5 FATIGUE IN COMPOSITE MATERIALS AND COMPONENTS

12.5.1 Axial Fatigue Strength of Open-Hole Specimens of T800H/PMR-15 Carbon/ Polyimide Composite at Room and High Temperatures

Y. Kakuta (JAXA), T. SHIMOKAWA, (TMIT), T. Tanimoto and J. Morishige (SIT), kakuta.yoshiaki@jaxa.jp

The objective of this study is to investigate the axial fatigue strength of a T800H/PMR-15 carbon/polyimide composite material at room and high temperatures. Open-hole specimens were machined from T800H/PMR-15 panels with a quasi-isotropic stacking sequence, 32 plies $(45/0/\text{-}45/90)_{4S}$.
The nominal thickness of the specimens was 4.29 mm, because this prepreg system was 0.134 mm thick.
Axial fatigue tests were conducted in a laboratory environment at room temperature (RT) and in an oven at 260°C under constant amplitude loading with a frequency of 10 Hz by using an electronic servo-hydraulic fatigue-testing machine. The stress ratios (R = minimum stress /maximum stress) were selected three kinds, i.e. 0.1 (tension-tension), 10 (compression -compression), and -1 (fully reversed). Prior to fatigue testing, specimens were kept in a thermo-hygrostat for 48 hours in order to control the moisture content of the specimens. The air in the thermo-hygrostat was adjusted to 23°C and 65% relative humidity.
Fatigue tests provided S-N relationships and fatigue failure modes at RT and 260°C. This study discusses the temperature effect on fatigue strength and fatigue failure modes.
Figure 12.9 presents the S-N relationships. The maximum stress in ordinate indicates the maximum stress for R = 0.1 and -1 and the absolute values of the minimum stress for R = 10. The least-squares method gave regression lines approximating S-N data on the basis of failure data only. When the slope of an S-N line was positive, a horizontal line was employed. Fatigue strengths for R and temperature combinations were compared at 10^5 load cycles, because most of the fatigue strengths at 10^5 cycles existed in the interpolated region of S-N lines. Figure 12.10 presents fractographs taken after fatigue failure. The pictures include surface and side views for failed specimens.
Major test results and conclusions are as follows:
Horizontal or almost horizontal S-N lines were obtained for the combinations of (R = 0.1, RT), (R = 0.1, 260°C), and (R = 10, 260°C). The slopes of other S-N lines were negative and very small. Therefore, the scatter of fatigue life was considered very large.
If compared with the fatigue strength at 10^5 cycles for RT, the fatigue strength at 10^5 cycles for 260°C decreased 19% for R = 0.1, 7% for R = 10, and 26% for R = -1. The reduction of fatigue strength was considered to be an effect of high temperature.

The failure modes did not change for the same R regardless of test environments of RT and 260°C. An axial splitting failure mode was observed for R = 0.1. However, for R = 10 and -1 a failure mode of a rhombus shape as a side view, dominantly caused by delamination buckling, was observed.

12.5.2 Fatigue Strength of Open-Hole Specimens of a G40-800/5260 Carbon/ Bismaleimide Composite Material at Room and Elevated Temperatures

T. Shimokawa (TMIT, E-mail: aero60jp@ybb.ne.jp), Y. Kakuta (JAXA), and T. Aiyama (Toyota Motor Corp.)

Carbon/bismaleimide composite materials are cost effective for use in medium-high temperature aircraft structures, because their prepreg price and processing cost are not so high in comparison with those of carbon/epoxy composite materials. However, fatigue data necessary to the design of aircraft structures, especially at elevated temperatures, are rarely available from published papers.

A G40-800/5260 was selected as a subject material of this study among carbon/bismaleimide composite materials available in the market. The stacking sequence of the laminates is 32 plies $[45/0/-45/90]_{4S}$**.** The nominal thickness of the specimens is 4.29 mm, because the prepreg is nominally 0.134 mm thick. Figure 12.11 shows the configuration of open-hole specimens tested.

Axial fatigue tests were conducted under constant amplitude loading at three kinds of stress ratio (*R*=minimum stress/maximum stress), tension-tension *R*=0.1, compression- compression *R*=10, and tension-compression *R*=-1, using a digital servo hydraulic material testing machine. Test environments were ambient air of room temperature (RT) and hot air of 150°C in an environmental chamber, where 150°C is expected to be the maximum allowable temperature. Fatigue loading speeds were 1 Hz and 5 Hz.

Fatigue test results are plotted on semi-logarithmic graph paper where the vertical axis is represented by the maximum absolute stress (MPa) and the horizontal axis is taken by logarithmic life. The fatigue data are approximated by a regression line on the graph. Figure 12.12 presents the results of tensile fatigue tests. Two unbroken data, ($S_{\max} = 615\,\text{MPa},\ \ N = 89,000$) and ($S_{\max} = 578\,\text{MPa},\ \ N = 1,000,000$), are included in the test results obtained at room temperature. The regression line is derived from the data including these two data. The *S*-*N* equations for the data at room temperature and 150°C are respectively given by

$$S_{\max} = -18.8 \log N + 713 \qquad (1)$$

and

$$S_{\max} = -18.7 \log N + 697\,. \qquad (2)$$

The slope is not changed for both temperatures and the intercept is a bit smaller at 150°C. The difference in the *S*-*N* relationships at room temperature and 150°C is very small as shown in Fig. 12.12.

Figure 12.13 presents the results of compressive fatigue tests, *R*=10. The *S*-*N* equations for the data at room temperature and 150°C are respectively given by

$$S_{\min} = -31.3 \log N + 508 \qquad (3)$$

and

$$S_{\min} = -18.5 \log N + 409 \,. \qquad (4)$$

The slope and intercept of Eq. (3) for the test results obtained at room temperature are a little higher than those of Eq. (4) for 150°C tests respectively.

Figure 12.14 presents the results obtained by tension-compression fatigue tests, *R*=-1. The *S*-*N* equations for the data at room temperature and 150°C are respectively given by

$$S_{\max} = -38.0 \log N + 507 \qquad (5)$$

and

$$S_{\max} = -31.2 \log N + 439 \,. \qquad (6)$$

The slope and intercept of Eq. (5) for the test results obtained at room temperature are a little higher than those of Eq. (6) for the test results at 150°C respectively.
The total compressive-stress amplitude in Eqs. (3) and (4) is 90% of $S_{\min}$, because *R*=10 was used in compression fatigue tests. Meanwhile, in case of tension-compression fatigue tests, that in Eqs. (5) and (6) is $S_{\max}$ because *R*=-1. In comparison of Fig. 12.13 and Fig. 12.14, almost equal total compressive-stress amplitude is calculated from Eqs. (3) and (5) at any number of load cycles *N* at room temperature. This situation is not changed for Eqs. (4) and (6) at 150°C. This fact demonstrates a very important phenomenon that the total compressive-stress amplitude dominantly affects the fatigue life in tension-compression fatigue tests.

12.5.3 Durability and Damage Tolerance Test of Co-Bonded CFRP Wing Structure

Yuichiro Aoki[a], Takashi Ishikawa[a], Shin-ichi Takeda[a],
Yuichi Hayakawa[b], Atsushi Harada[b] and Hiroshige Kikukawa[c]

[a] Japan Aerospace Exploration Agency, 6-13-1 Osawa, Mitaka, Tokyo 181-0015, Japan
[b] Fuji Heavy Industries Ltd., 1-1-11 Yonan, Utsunomiya, Tochigi 320-8564, Japan
[c] Japan Aircraft Development Corporation, 1-2-3 Toranomon, Minato-ku, Tokyo 105-0001, Japan

Weight reduction and lower production costs are important goals for aircraft structural engineers and researchers. In recent years, the use of advanced composite structures has increased to realize these goals. JAXA (Japan Aerospace Exploration Agency) is conducting various tests and establishing evaluation technologies for adequate verification of the structures. This research is carried out by JAXA, led by JADC (Japan Aircraft Development Corporation) and sponsored by NEDO (New Energy and Industrial Technology Development Organization). In this paper, fatigue tests of a stiffened panel were reported, where this panel is a typical part of the upper skin of a lightweight composite wing made by new processing technology.
The test panel was designed and fabricated by FHI (Fuji Heavy Industries, Ltd.), which is a portion of the upper skin of a wing of a small-sized jet transport [1, 2]. A general view of the panel is shown as Fig.12.15. Novel and unique structural concepts were adopted to simulate for the fabrication of the panel.

First stage Resin transfer Molding (RTM)-cured stringers were co-bonded onto the raw layered skin. Each hat-shaped stringer is reinforced by stitched fiber in order to provide better damage tolerance. For the gripping of the panel with actuators, steel fixtures are attached to both ends of the panel by fasteners.

Figure 12.16 shows test procedures and check items. All the test equipment and devices were checked at a low load level prior to impact test. Impact damages were given by a drop-weight impact machine with a 5/8 inch hemispherical top. Impact energies, locations, and directions are shown in Fig.12.17. BVIDs (Barely Visible Impact Damages) were first introduced to points A and B of the panel. Each point is located at a skin/stringer co-bonded part and a typical skin part of the panel, respectively. A spectrum loading was applied to the panel with BVIDs for a period of the twice design life to verify durability and damage tolerance. The VID (Visible Impact Damage) was then given at point C of the panel. After VID was introduced, a damage growth test was conducted by the spectrum loading to a design life. The purpose of this test is to demonstrate that a detectable damage would not increase to a detrimental size during an inspection interval. NDI (Non-destructive inspection) was carried out every 1/10 of the design life during tests for the evaluation of the increased impact damages. Pulsed thermography was used as a main tool for NDI, because it is quick and easy to use. Ultrasonic C-scanning system was used in order to compare with the inspection results before and after the tests. Finally, static load was applied up to design limit load for verification of the residual strength after fatigue tests.

All the spectrum loading tests were performed by the Mini-TWIST [3, 4], which is the European standard gust load sequence for flight simulation tests on transport aircraft structures. Mini-TWIST represents a load sequence for a block of 4,000 flights composed of 10 distinct flight types (A to J). Load levels in each flight have been normalized by a 1G mean level during cruise conditions. The highest peak load level is 2.6G, which occurs only once in the total sequence. In present tests, 40,000 flights were fixed one design life, and mean load level (1G) was -171 kN because of the compressive condition dominant in the upper skin of the wing.

The load was applied to the panel through a hydraulic testing machine MTS-880 of 500 kN capacity. Loading signals were generated in a control system MTS-Flex Test SE. A Multi-channel data logger was used as one of the data acquisition devices for 1 channel of load and 63 channels of strains. In fatigue tests, the channel of load and 6 channels of higher strain outputs were recorded during loadings, and all the strain outputs were recorded during the most severe flight, the A-type flight. The other data acquisition systems were an AE data analyzer of 7 channels and a structural health monitoring system using FBG (Fiber Bragg Grating) sensors near impact points.

Figure 12.18 shows examples of measured data histories in an A-type flight. Each figure depicts load, two selected strains, and relative displacement between loading grips. In the first fatigue test, the maximum compressive strain of 3100 $\mu\varepsilon$ at the highest peak load appears near the impact point A of the internal side of skin. Figure 12.19 illustrates a comparison of delamination shapes of BVIDs before and after an 80,000-flight fatigue test. The inspection results were obtained from pulsed thermography and ultrasonic c-scanning system. The results verify that BVIDs have not grown through the fatigue test. The VID inspection results during the damage growth test are shown in Fig.12.20. VID delamination growth has not been detected in the test. The maximum compressive strain at the highest peak load was found to be 3700 $\mu\varepsilon$ near VID. AE signals were mainly generated around fasteners of end fixtures during the tests. It is found that the BVID was not a significant source. Damages were not detected by the FBG sensors. In the final residual strength test, the load bearing-capability of the present panel with BVID and VID was verified at design limit load level. In conclusion, excellent fatigue and damage tolerance properties of the present structure were verified and demonstrated. No damage growth was observed during spectrum fatigue loading over three times of the design life.

References
1)Y. Toi, et al., Proceedings of. 7th Japan International SAMPE Symposium, 2002, 145-148.
2)Y.Hayakawa, et al., Proceedings of. 8th Japan International SAMPE Symposium, 2003, 1291-1294.
3)J. B. de Jonge, et al., NLR TR 73029 U, 1973.
4)H. Lowak, et al., NLR MP 79018 U, 1979.

12.5.4 Development and Substantiation of Innovative Composite Wing

M.Hiraki, S.Tanaka, A.Harada and Y.Toi, Fuji Heavy Industries LTD. (FHI)

In WISTR (Wing Innovative STRucture) program, unique and innovative composite wing box structure by “3 in 1 Co-bond process” with advanced technologies including VaRTM/RTM methods has been developed. For substantiation, various tests are conducted to verify that design and manufacturing process comply with FAA 14 CFR Part25. Sub-component test which verifies flaw growth behavior and full-scale test for static and residual strength have shown damage tolerant capability of newly proposed structure.
The unique structure as shown in Figure 12.21 has been selected from studies of optimum design as integral fuel tank wing of small transportation jet. This wing box structure is assembled from major 3 parts which are lower box, upper panel and rib webs. Lower box is co-bonded as one large part with low temperature initial-cured VaRTM(Vacuum Assisted Resin Transfer Molding) stringers and RTM(Resin Transfer Molding) spars and raw prepreg skin. This process is very unique and affordable process called “3 in 1 Co-bond”. It means three processes are completed at one auto-crave cure, curing of VaRTM/RTM parts, bonding parts and curing prepreg of skin. Figure 12.22 shows full-scale fabrication try for process and tool qualification.
As substantiation, coupon tests for material properties, element tests for allowables and structural tests have been conducted per compliance matrix defined as shown in Table 1, based on MIL-HDBK17-1F, FAA 14 CFR Part25, AC20-107A. Structural tests have been planned to verify damage tolerant capability especially focused on co-bonding strength. Sub-component test of 3-stringer panel has been conducted in JAXA (Japan Aerospace Exploration Agency). BVID (Barely Visible Impact Damage) and VID (Visible Impact Damage) were applied to the panel to verify flaw growth behavior and test results showed no-flaw growth property and enough residual strength after cyclic loading.
Full-scale test has been conducted to validate static and residual strength. The test fixture is simplified to realize critical load distribution in critical area. The test sequence consists of several cases, static and residual strength verification as shown in Figure 12.23. Damages tabulated in Table 2 were applied to the test article for each requirement. To evaluate static strength, 3 BVIDs were applied to typical area of the structure as damages in operation and manufacturing. Internal damage was around 20 mm-diameter by Non-Destructive-Inspection. To evaluate residual strength up to design limit load VID was applied to skin-stringer co-bond area. Internal damage was 45 mm diameter and damage was clearly visible with 0.2 mm depth. As discrete source damage, large notch was applied which simulates uncontained fan blade impact since it was the critical failure mode of this structure. The structure with discrete source damage has to withstand get home load set as 70% limit flight maneuver loads. The test results have been met each requirement as shown in Table 3. Then the load was applied to the structure up to failure for validation of the analysis method. It was proved that the actual failure load was higher than the prediction as shown in Figure 12.24 and the analysis method is valid for this innovative structure.
As mentioned above, this unique and innovative wing box structure with “3 in 1 Co-bond” process has been substantiated to have enough damage tolerant capability complied with FAA 14 CFR Part25.
The authors wish to acknowledge the New Energy and Industrial Technology Development Organization (NEDO) and Japan Aircraft Development Corporation (JADC) for the financial and technical support to this research program on innovative wing structure.

12.5.5 Residual Strength for A-VaRTM structural elements

T. Sakagawa and Y. Komori, Mitsubishi Heavy Industries, Ltd. (MHI)

It is well known that VaRTM (Vacuum-assisted Resin Transfer Molding) is an attractive fabrication process not requiring expensive autoclave. This fabrication process results in not only low cost production but also eliminating product's size limitation due to autoclave. Currently, one of the key issues about VaRTM to be proved is that mechanical properties of composite fabricated by VaRTM are equivalent to those of traditional pre-impregnated materials. Mitsubishi Heavy Industries, Ltd. (MHI) and Toray Industries, Inc. (Toray) have been jointly developing new VaRTM process as well as materials, which are named "A-VaRTM" (Advanced VaRTM)", aiming for application on aircraft primary structures.

Typical structural elements – 3-stringer panel specimen:

To assess the possibility of A-VaRTM application on aircraft primary structure, residual strength tests using 3-stringer co-bonded panel (1m long) were conducted as a typical element (Figure 12.25). Co-bonded panel (with pre-cured skin) instead of co-cured one was used to avoid possible risks by resin infusion problem (insufficient fill) onto co-cured surface and part dimensional accuracy, even if MHI will pursue the co-cured (more costly effective) process on future aircrafts. As a result, 3-stringer co-bonded panel by A-VaRTM has constantly over-55% Vf (volume of fiber), good dimensional accuracy and also good internal-part quality without void or resin rich area.

Impact damage applied on specimen:

Currently, A-VaRTM composite consists of intermediate modulus carbon fibers (T800S) with thermoplastic toughening particles and 180℃ cure epoxy resin system. According to MIL-HDBK-17 or other documentation, 136J(100ft-lb) was applied on skin of 3-stringer panel as cut-off energy of impact damage (Figure 12.26).

Residual strength test result:

Compression test for the 3-stringer panel with 136J cut-off energy impact on the skin was conducted. Actual compressive modulus with impact damage is 64.3GPa compared with 65.9GPa estimated by lamination theory. Thanks to toughened resin matrix, this 3-stringer panel has high redundancy against impact damage. Also, final compressive strain to fail is over 4,200-micron (to our target 4,000 micron-strain) (Figure 12.27).

Conclusion:

New material/process of A-VaRTM demonstrates competitive compressive strength even after cut-off impact energy. MHI will pursue the possibility of A-VaRTM application on brand new regional jet structure and also improve not only material and process but also design for realizing large and high-loading aircraft primary structure in future.

12.5.6 Full-Scale Component Tests of Composite Wing Control Surfaces – EMB190

K. Toyoda, H. Sashikuma and T. Taki, Kawasaki Heavy Industries, Ltd. (KHI)

Kawasaki Heavy Industries, Ltd. (KHI) is participating in the development of EMB190 as a risk sharing partner and is developing most of wing structure as well as EMB170.

We have been carrying out three full scale component tests of wing control surfaces in parallel from 2004 to2005 at Gifu Works, KHI in Japan for type certification. The tests consist of three structural strength tests for Inboard Flap, Outboard Flap and Aileron.

Figure 12.28 shows KHI's work share and component test items. Figure 12.29 shows the photographs of full scale component tests of wing control surfaces.

In this paper, the structural strength test of Inboard Flap is presented as a representative.

Structural strength test of Inboard Flap

The flap is double slotted type and consists of main flap panel, aft flap panel and mechanism. The flap panels are mainly made of 180^{o}C cure carbon/epoxy composites material, KMS-6115. (KHI developed KMS-6115, which is a carbon/epoxy pre-preg for aircraft primary and secondary structures. This material was approved by JCAB, CTA, JAA and FAA.)

The test fixture consists of a loading fixture (whiffletree), support fixture, environmental chamber and so on. The test loads are introduced into the lower surface of the flap panels with rubber pads in order to simulate the design load distribution. Three hydraulic actuators and whiffletrees are used to introduce static loads and fatigue load spectrum.

One test specimen (LH part) is used for the static and fatigue test. "No growth design concept" is applied to the flap composite structure for the damage tolerance substantiation.

The test procedure is as follows.

1) Test specimen manufacturing - Introduction of maximum fabrication defects and cosmetic repair simulation
2) Introduction of visible damages
3) Moisture pre-conditioning up to design moisture content
3) Limit load test in high temperature/wet condition
4) 2 lifetime fatigue test in operational temperature/wet condition – Flight by flight load with fatigue load enhancement factor
5) Ultimate load test in high temperature/wet condition
6) Overload test in high temperature/wet condition

This structural strength test of Inboard Flap, as well as Outboard Flap and Aileron, has been completed in March 2005. And EMB190 regional jet will be approved by CTA in this summer.

12.5.7 Application of 3-D Woven Composites to Aircraft Fitting Structures

H. Kawakami and M. Kageyama, Third Research Center, Technical Research and Development Institute (TRDI), Japan Defense Agency

Full scale component tests of fittings made of three-dimensional woven composite materials were completed successfully at the TRDI third research center in early 2004. These tests are composed of static test, two life times fatigue test, residual strength test and tear down inspection, and were regarded as final evaluation in the project which started in 1989 for the acquirement of 3-D composite technology.

The test specimens were designed for typical military fighter aircrafts and manufactured by resin transfer molding (RTM). The specimens consist of wing root fittings, fuselage carry-through fittings, horn fittings, actuator rods and cylinders as shown in Figure 12.30. Primary fibers of composites are oriented toward 0/±45/90 with respect to in-plane and through the thickness, and additional fibers, such as hoop directed fibers in the local regions around open holes, were arranged in consideration of individual characteristic of specimens.

The fatigue tests were conducted for two life times under the hot temperature and wet (HTW) condition. Test spectrum were based on that of typical fighter aircraft and loaded with random program except for low-high block program of the actuator specimens. After the completion of fatigue test and residual strength test, the structural tear down inspection was done.

In all tests the behaviors of 3-D composite fittings were as expected analytically. No significant fatigue or environmental degradation instances in all test specimens was emerged. The difference of both failure mode and load between static and fatigue test specimens was not observed at all.

12.5.8 SH-60J KAI Main Rotor Blade Full Scale Component Fatigue Tests

H. Kawakami and M. Kageyama, Third Research Center, Technical Research and Development Institute (TRDI), Japan Defense Agency

The fatigue tests, including fractography inspections, of the SH-60J KAI rotorcraft main rotor blade (MRB) had been successfully carried out on March 2003, and then the evaluation of test results was completed in September 2003.

The fatigue tests were conducted by using the specimens of three segments cut from the full scale MRB: an inboard, outboard and tip component specimen. The advantages are:

- Space-saving and simplification of test instruments
- Shortening of test duration because of conducting tests for three segments in parallel and optimization of test settings for their individual test requirements

The test loads were divided into in-flight high-cycle fatigue loads and ground air ground (GAG) low-cycle fatigue load, which consist of the centrifugal force, flapping moment, edgewise bending moment and feathering torque. The in-flight tests were applied to all of three component specimens, in other hand the GAG test was done for only inboard one. Figure 12.31 shows schematic view of the test specimens and instruments.

12.6 FULL-SCALE FATIGUE TESTING

12.6.1 US-1A KAI Full Scale Static and Fatigue Test

H. Kawakami and M. Kageyama, Third Research Center, Technical Research and Development Institute (TRDI), Japan Defense Agency

This review provides the current status and several topics of the full scale static and fatigue test (FSST & FSFT) program of US-1A KAI aircraft. The development of the US-1A KAI, Japanese new search and rescue amphibious aircraft, was started in 1996 for the Japan Maritime Self Defense Force (JMSDF) as reported in the previous ICAF reviews. The various modifications from the current US-1A aircraft, such as the pressurized cabin, replacement of engines and increase of aircraft weight, require the full scale static and fatigue test. The ground full scale structural tests and the flight test will be accomplished in 2006.

The full scale static test (FSST) was also started in December 2002 by the TRDI third research center. Up to now most of load cases were completed without any critical failure in the primary structures. The remaining several ultimate load tests continue till March 2005.

The FSFT was started in January 2004 by the TRDI third research center. The durability test of two life times was completed in late 2004, and now the inspection of test article and the preparation for the damage tolerance test of another two-life-time loading are under way. The main characteristics of the FSFT are as follows:

- Full aircraft including complete fuselage, main wing and landing gears with dummy vertical and horizontal stabilizers (see Figure 12.32 and 12.33)
- Integration of landing gear fatigue test into the FSFT
- Flight by flight random loading with several missions
- More than 150 hydraulic actuators to simulate air, inertia and water loads, and air compressors to simulate cabin pressure.

The water impact loads during takeoff and landing are quite important for the US-1A KAI which has the capability to land on the water under the wave height of 3 meters condition. The estimation of the water load is a complex problem, since it needs to take into account stochastic factors like wave conditions and poorly predictable factors like dynamic response of aircraft structures. Therefore the distribution and the frequency of water loads are established based on the appropriate combination of related MIL specifications, the service load experience in the current US-1A aircraft and the result of the rational analysis on hydraulic characteristics.

The particular shape of amphibious aircraft hull structures and the large compression loadings of water impact results in the instability behavior which is the same phenomenon as an inverted pendulum (see Figure 12.34). The divergence from small irregularity of loading or article position occurred because of this instability, and was one of the bottlenecks of the FTFS as well as the FSST. This behavior is now handled by the adjustment of local loading sequence and the introduction of the position control system which compensates for the six degrees of freedom of the test article by means of small additional loadings.

12.6.2 P-X/C-X Full-Scale Structural Strength Test

H. Kawakami and M. Kageyama, Third Research Center, Technical Research and Development Institute (TRDI), Japan Defense Agency

TRDI has developed the P-X, the Japanese next generation maritime patrol aircraft, and C-X, the next generation cargo transport aircraft, as the successor aircraft to the current P-3C and C-1 respectively. The main feature is the utilization of the merit of simultaneous development of two aircraft, in order to reduce life-cycle-cost. That is the common use of some structural parts, such as outer main wings and horizontal stabilizers, and some equipment, such as integrated display units and inertial reference units and so on. The full scale structural strength tests of both aircraft are planned to start in 2006.

12.7 FATIGUE MONITORING

12.7.1 Structural Health Management of Smart Composite Structures Using Small-Diameter Fiber Optic Sensors

Nobuo Takeda, The University of Tokyo, takeda@smart.k.u-tokyo.ac.jp

The small diameter optical fibers (both single-mode and multi-mode) were developed and FBG (fiber Bragg grating) sensors were fabricated with these optical fibers. The optical fiber is with 40 μm in cladding diameter and 52 μm in polyimide coating diameter, which is easily embedded within one CFRP ply of typically 125 μm in thickness. Such optical fibers have both mechanical and optical properties similar to those of conventional optical fibers with 125 μm in cladding diameter and do not cause any reduction in strength of composites when embedded parallel to reinforcing fibers in laminates. Then, FBG sensors were also successfully developed with these single-mode small-diameter optical fibers, where periodic gratings with approximately 0.53 μm in space were inscribed in the gage section (typically 10 mm in length). FBG sensors are usually used to measure strain and/or temperature through the shift of the wavelength peak of the reflected light.

However, FBG sensors are also very sensitive to non-uniform strain distribution along the entire length of the grating, and that the small-diameter optical fibers enable us to embed the FBG gage section near the location where the damages might occur in the laminate. When an FBG sensor was embedded in the -45^o ply to detect transverse cracks in the adjacent 90^o ply of CFRP quasi-isotropic laminate $[45/0/-45/90]_s$ (Fig. 12.35), a non-uniform strain distribution due to the initiation and evolution of transverse cracks caused the wavelength distribution in the reflected light, as shown in Fig. 12.36 [1]. While there were no transverse cracks, the spectrum kept its shape and the center wavelength shifted corresponding to the applied strain. With increasing transverse crack density, the shape of the reflection spectrum was distorted; the intensity of the highest peak became small, some peaks appeared around it, and the spectrum became broad. These experimental observations could be well explained by the theoretical prediction using the calculated strain distribution and the fiber optic theory.

In the “R&D for Smart Material/Structure System (SMSS)” project (October 1998 to March 2003) in Japan, a composite fuselage demonstrator for damage detection and suppression was fabricated. Figure 12.37 shows the final assembly with 3 m in length and 1.5 m in diameter. In the upper panel of the Damage Detection and Suppression Demonstrator, the small-diameter optical fiber sensors were embedded in order to detect impact-induced damages (Fig. 12.38). The fiber connecters had been well designed to be embedded so that the fabricated CFRP panel could be trimmed at the edges after the manufacturing for practical use. The small-diameter FBG sensors were used to obtain the impact location through the dynamic strain measurement, and multi-mode small-diameter optical fibers were embedded to judge the occurrence of the impact-induced damages using the optical loss due to bending. An impact detection and localization system was also developed which could successfully detect the impact locations and impact-induced damages [2].

REFERENCES

1. T. Mizutani, Y. Okabe and N. Takeda, Quantitative evaluation of transverse cracks in carbon fiber reinforced plastic quasi-isotropic laminates with embedded small-diameter fiber Bragg grating sensors. *Smart Mater. Struct.*, **12**(6), 898-903 (2003).
2. H. Tsutsui, A. Kawamata, J. Kimoto, A. Isoe, Y. Hirose, T. Sanda and N. Takeda, Impact damage detection system using small-diameter optical fiber sensors embedded in CFRP laminate structures, *Adv. Comp. Mater.*, **13**(3), 3-5 (2004).

12.8 AIRCRAFT ACCIDENT INVESTIGATION

12.8.1 Aircraft Accident Investigation and Aircraft Serious Incident Investigation

Hiroaki Tomita, Aircraft and Railway Accidents Investigation Commission (ARAIC)
e-mail:kumakura-y25e@mlit.go.jp

(1) *Total number of registration in Japan*

As of December 31, 2004, the number of civil aircraft registered in Japan was 2,678 including 1,216 airplanes (of which 610 were reciprocating engine airplanes), 802 helicopters, 658 gliders including motor gliders and 2 airships.

(2) *Statistics in relation to the accident and serious incidents investigation*

The numbers of accidents and serious incidents that the ARAIC has investigated during past 2 years are shown in Table 12.4 and 12.5. The accident investigation and serious incident reports were issued for 76 in 2003 and 2004. The causal factors for 50% of these accidents were related to pilots, 23% to mechanical failure and 27% to weather or others.

(3) *Accident examples of fatigue failure*

a) The motor glider, VALENTIN Model TAIFUN 17EII lost its propeller just after takeoff.

The mechanic, who had installed the propeller, had inserted an O-ring that must not install between the propeller hub and the propeller flange.

Therefore the hub and the flange could not adhere, the stud bolt was struck the repeat load that wasn't assumed and the stud bolt had broken off by the fatigue.

The numbers of beach marks of fractured surface of stud bolt agreed with the flight cycles after propeller installed.

b) One of the fan blades of No.2 engine of Boeing 747-200B from approximately 19 cm outboard of the platform had broken off in flight.

Examination of the fracture surface of fan blade found beach marks, indicative of fatigue fracture.

A small area of the trailing edge of fan blade was melted by arc burn, and as it re-solidified rapidly in the air a brittle region with changed microstructure was created. The brittle region was subsequently damaged, and a crack initiated in the damaged area.

12.9 ICAF DOCUMENTS DISTRIBUTED BY JAPAN DURING 2003 TO 2005

2353 Statistical analysis for application of the Paris equation to whisker reinforced metal matrix composites (J. J. Ahn and S. Ochiai)

2354 Effect of surface roughness on step-wise S-N characteristics in high strength steel (H. Itoga, K. Tokaji, M. Nakajima and H.-N. Ko)

2355 The effect of second principal stress on the fatigue propagation of mode I surface crack in Al_2O_3/Al alloy composites (S. Kitaoka and Y. Ono)

2356 Fatigue behavior and fracture mechanism of a 316 stainless steel hardened by carburizing (K. Tokaji, K. Kohyama and M. Akita)

2357 Fatigue crack propagation and local crack-tip strain behavior in TiNi shape memory fiber reinforced composite (A. Shimamoto, H. Y. Zhao and H. Abe)

2358 Stress intensity factor analysis and fatigue behavior of a crack in the residual stress field of welding (H. Terada)

2360 Statistical fatigue properties in the large strain region of a stainless sheet for use as an abrasion strip on helicopter rotor blades (T. Shimokawa, Y. Hamaguchi, S. Machida, T. Ogawa and H. Itabe)

ACKNOWLEDGMENTS

Dr. Shinji Ogihara, Associate Professor Tokyo University of Science is greatly appreciated for his elaborate preparation shown during the course of compilation of present national review.

TABLES AND FIGURES

Table 12.1 Compliance Matrix for Wing Box

AC20-107A Paragraph		Substantiation Method						
		Design Data	Analysis	Test				
				Coupon	Element	Sub-component	Full-scale	Flight
Material & Fabrication Process				◎	◎		◎	
Proof of Structure	Static		◎	◎	◎	◎	◎	
	D&DT				◎	◎	◎	
	Flutter		◎				◎	○
Additional Consideration	Impact dynamics	◎	◎			○	○	
	Flammability	◎			○			
	Lightening Protection	◎	○		○	○		
	Protection of Structure	◎		○	○			
	Quality Control	◎			◎			
	Production Spec	◎			◎			
	Inspection and maintenance	◎	○		○	○		
	Substantiation of Repair	◎	○		○	○		

◎ : Conducted in WISTR program

○ : Need for actual program

Table 12.2 Applied Damage Data

Damages	Requirement	Location	Occasion	Diameter of Impactor	Internal Damage Diameter	Dent Depth
BVID (Barely Visible Impact Damage)	Design Ultimate Loads	Upper skin/ Stringer bonding Area	Impact Damage in operation	Φ 25.4 mm	18 mm	0.10 mm
		Upper skin	Impact Damage in operation	Φ 25.4 mm	15 mm	0.051 mm
		Front Spar Web	Impact Damage Manufacturing	Φ 12.7 mm	22 mm	0.025 mm
VID (Visible Impact Damage)	Design Limit Loads	Upper skin/ Stringer bonding Area	Impact Damage in operation	Φ 25.4 mm	45 mm	0.20 mm
DSD (Discrete Source Damage)	70% limit flight maneuver loads	Upper skin	Uncontained fan blade impact	Notch length: Stringer Pitch Notch Width: 7 mm		

Table 12.3 Test Results of Full-scale test

Test Case	Requirement	Test Results	Authority
Deformation	The structure must be able to support limit loads without detrimental permanent deformation.	Test results showed no detrimental permanent deformation	FAR 25.305 (a)
Static Strength with BVID	The Structure must be able to support ultimate loads without failure for at least 3 seconds.	Test results showed no failure for at least 3 seconds.	FAR 25.305 (b)
Residual Strength with VID	The residual strength evaluation must show that the remaining structure is able to withstand the loads.	Test Article withstanded required loads (Design Limit Loads)	FAR 25.571 (b) AC 20-107A
Residual Strength with DSD	The airplane must be capable of successfully completing a flight during which likely structural damage occurs as a result of Uncontained fan blade impact;	Test Article withstanded required loads (70% limit flight maneuver loads)	FAR 25.571 (e) AC 25.571-1C
Failure load Verification	(Verify failure load compared with the prediction by analysis)	Failure an 148% of design limit loads. Prediction was 138% of design limit laods.	

Table 12.4 Number of Accidents investigated in Japan for past 2 years

Aircraft type	Airplane	Helicopter	Glider and Motor glider	Others (ULP etc.)	Total
2003	12	1	2	3	18
2004	15	6	3	3	27

Table 12.5 Number of Serious incidents investigated in Japan for past 2 years

Aircraft type	Airplane	Helicopter	Glider and Motor glider	Others (ULP etc.)	Total
2003	8	2	1	4	15
2004	8	2	0	4	14

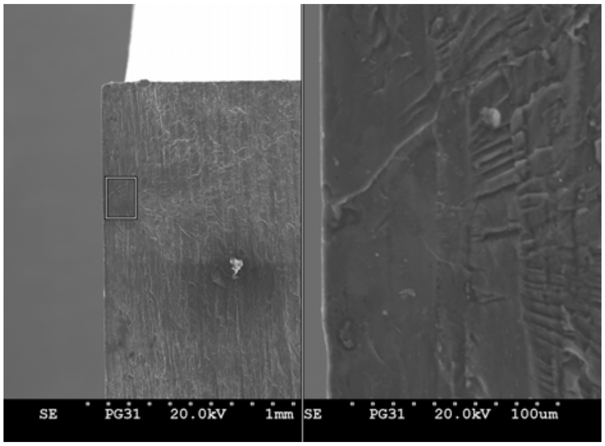

Fig. 12.1 Small corrosion pit as origin of fracture surface

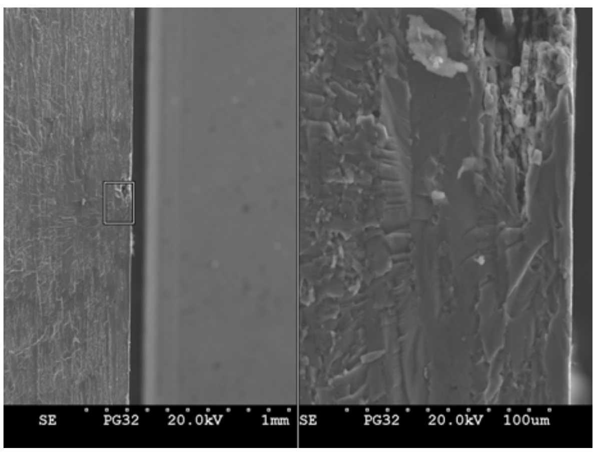

Fig. 12.2 Large corrosion pit as origin of fracture surface

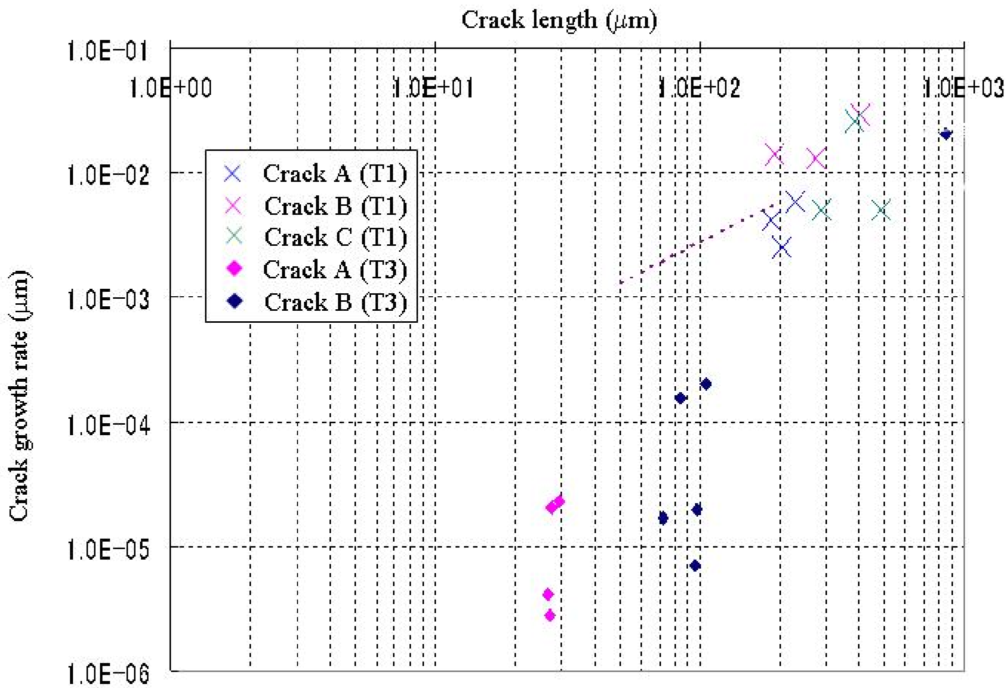

Fig. 12.3 Relationship between crack length and crack growth rate

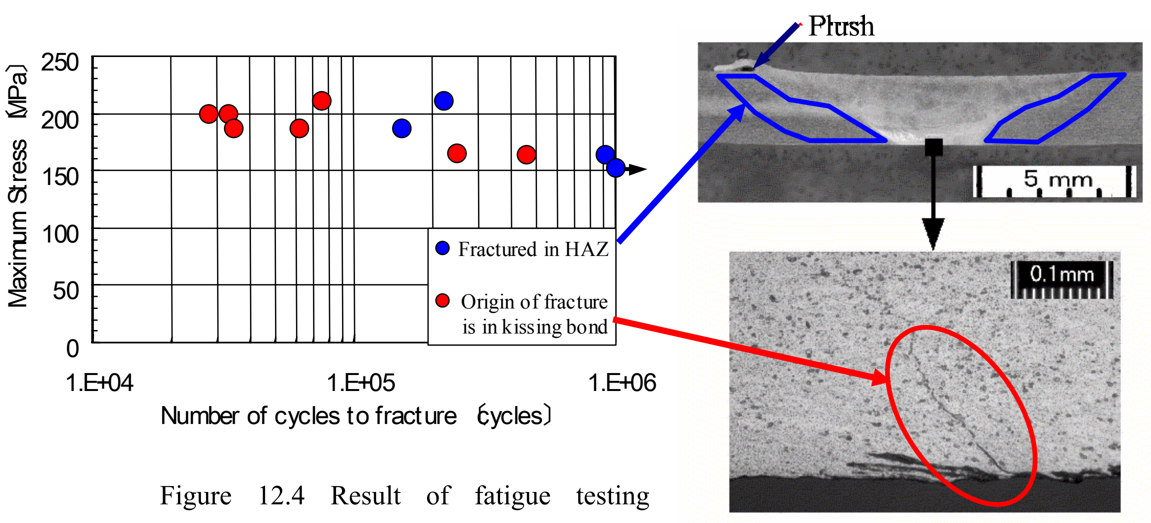

Figure 12.4 Result of fatigue testing regarding the effect on kissing bond

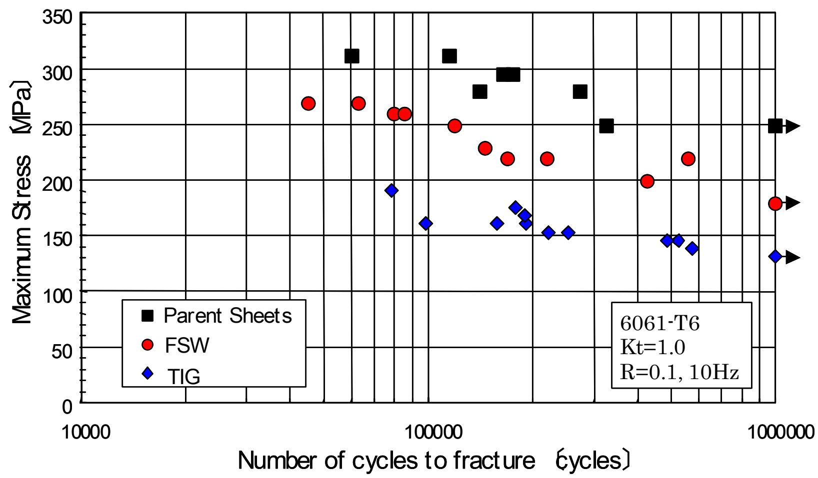

Figure 12.5 Results of the fatigue tests carried out on parent sheets and welded specimens. (6061-T6)

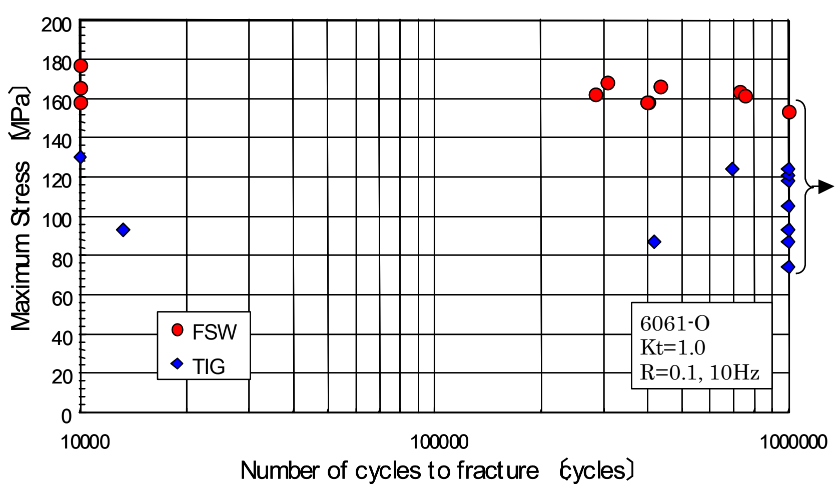

Figure 12.6 Results of the fatigue tests carried out on welded specimens.(6061-O)

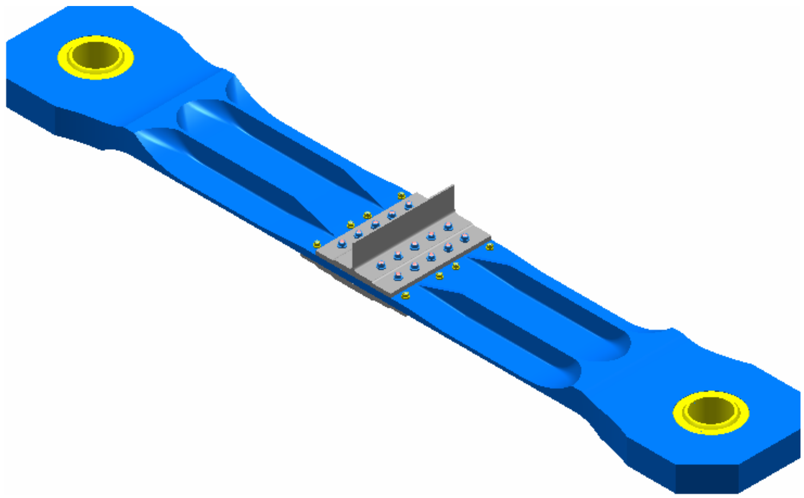

Figure 12.7 Joint element test specimen (Type 1)

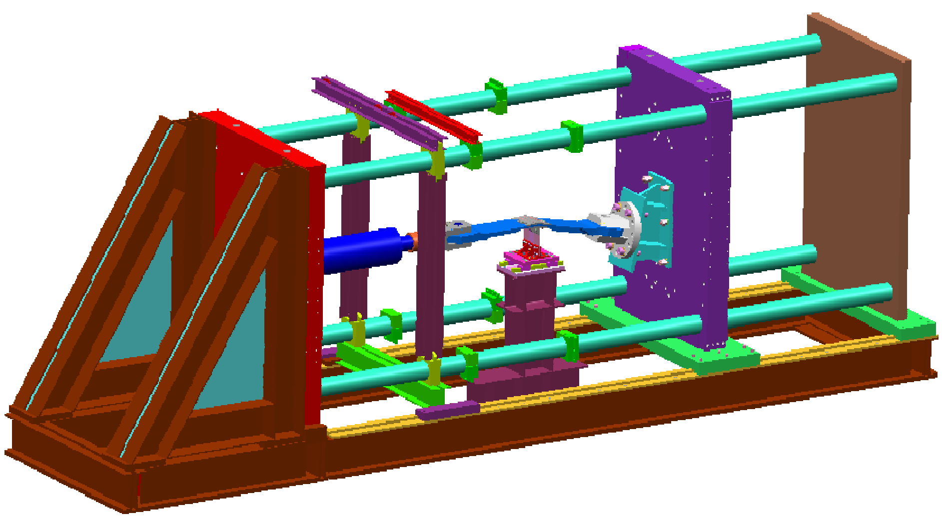

Figure 12.8 Test setup of type 2 specimen

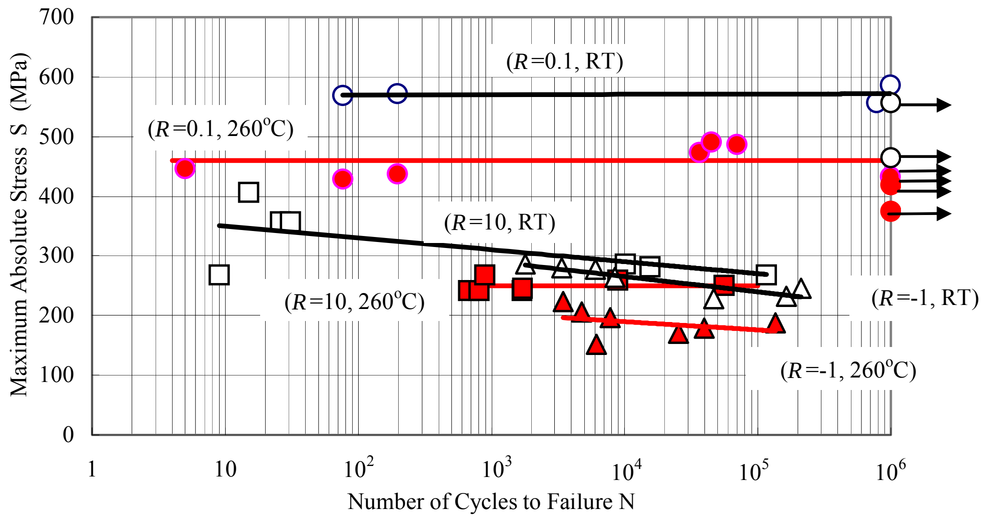

Figure 12.9 S-N relationships of open-hole specimens of T800H/PMR-15 carbon/polyimide composite for three stress ratios, R, at room temperature (RT) and 260°C.

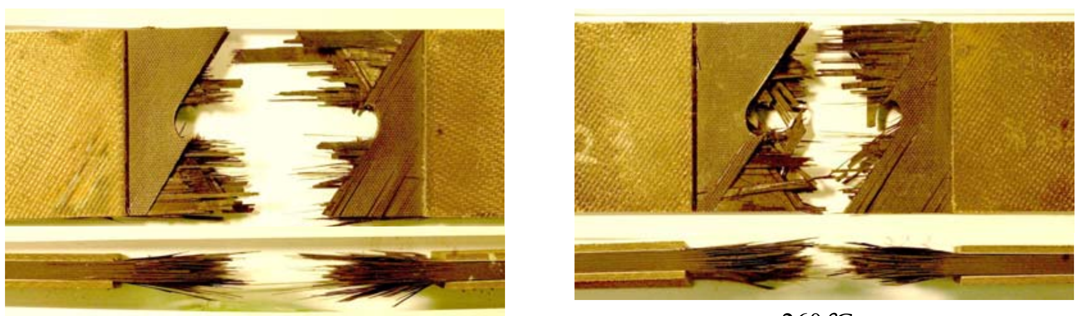

RT 260℃

(a) Loading condition*R* =0.1

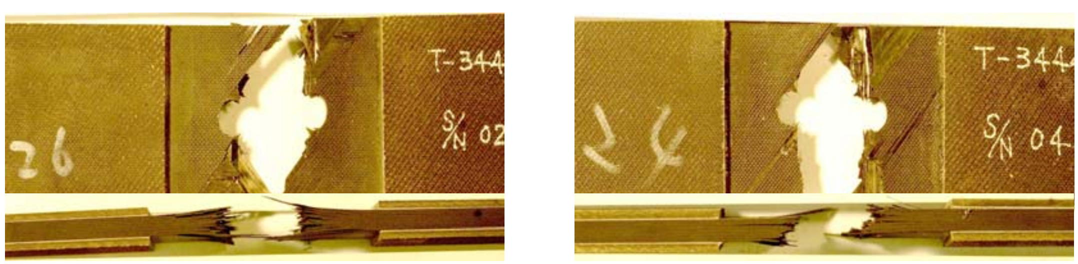

RT 260℃

(b) Loading condition *R* =10

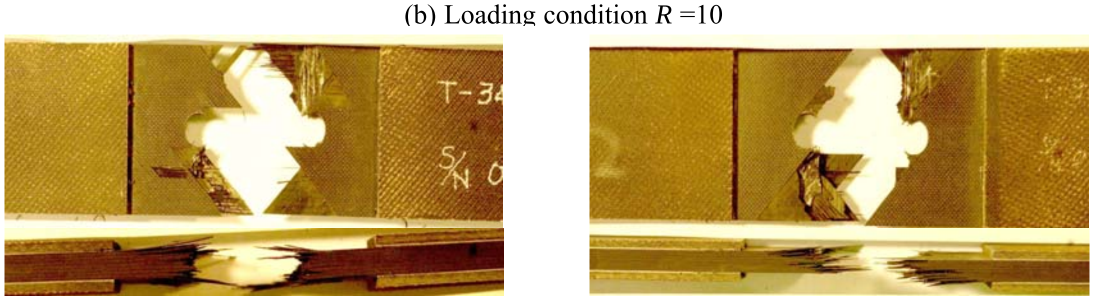

RT 260℃

(c) Loading condition *R* = -1

Figure 12.10 Fractographs taken after fatigue failure for the combination of three loading conditions and two temperature environments.

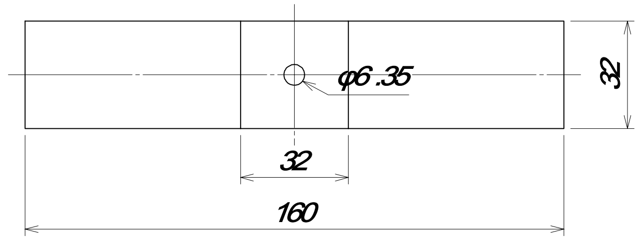

Figure 12.11 Specimen configuration.

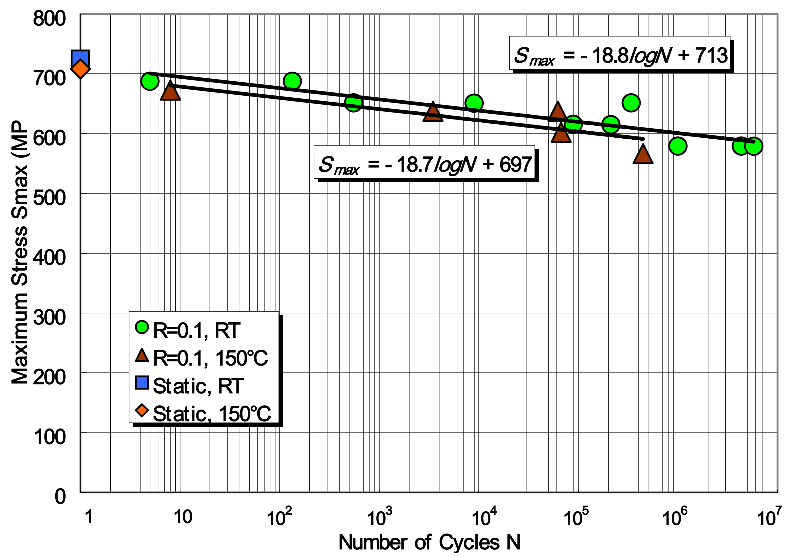

Figure 12.12 *S-N* relationships of open-hole G40-800/5260 specimens for tensile fatigue tests, *R*=0.1, at room temperature and 150°C.

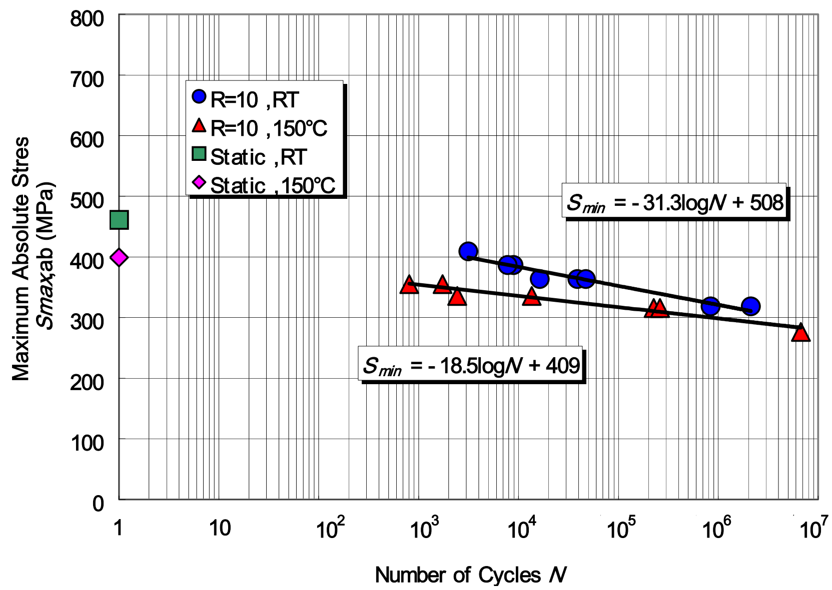

Fig. 12.13 *S-N* relationships of open-hole G40-800/5260 specimens for compressive fatigue tests, *R*=10, at room temperature and 150°C.

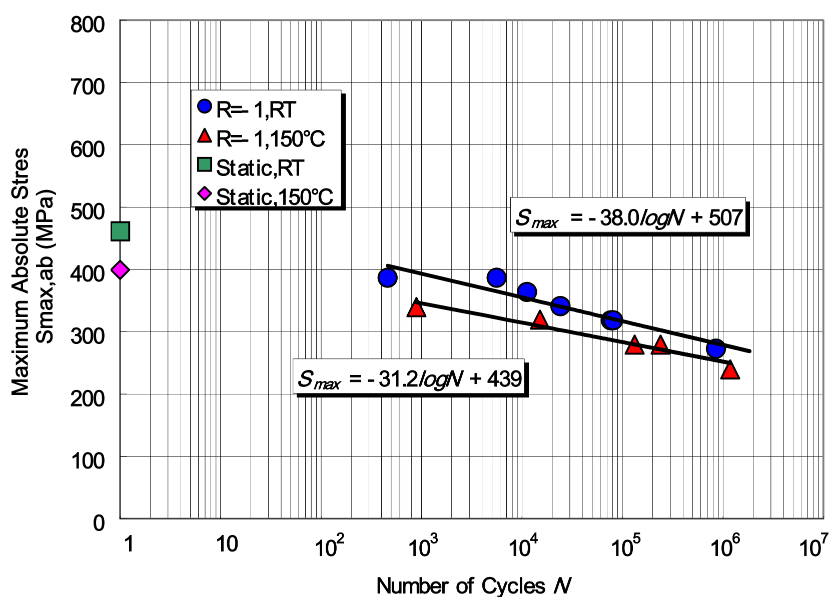

Fig. 12.14 *S-N* relationships of open-hole G40-800/5260 specimens for tension- compression fatigue tests, *R*=-1, at room temperature and 150°C.

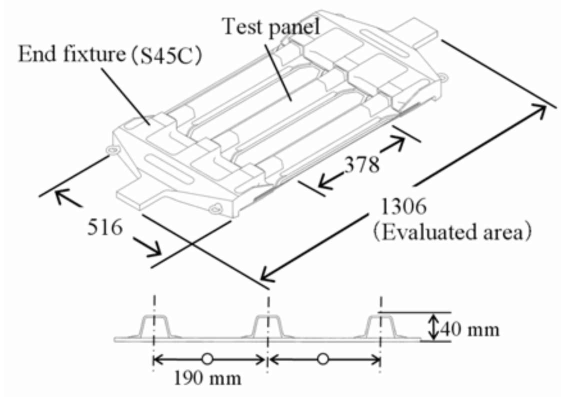

Figure 12.15 Schematic view of test

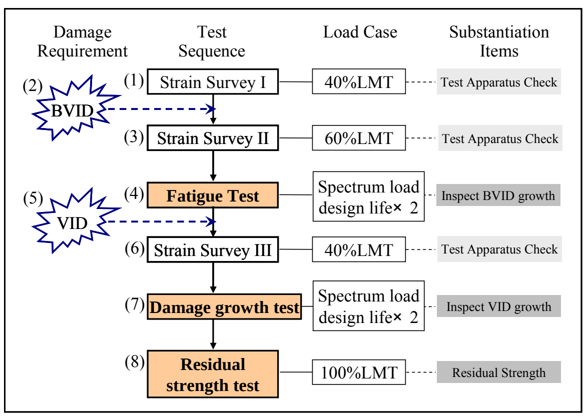

Figure 12.16 Test sequence and items.

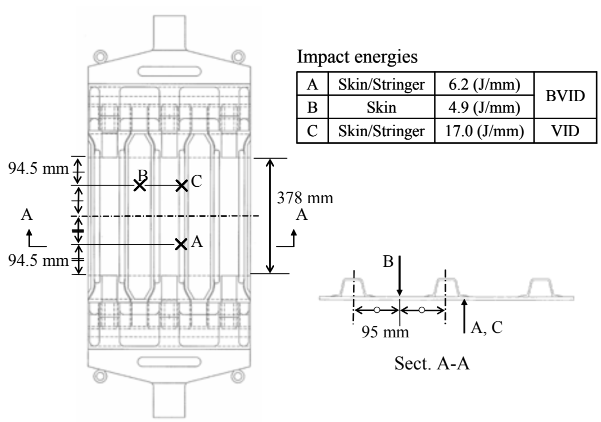

Figure 12.17 Overview of test panel and impact points.

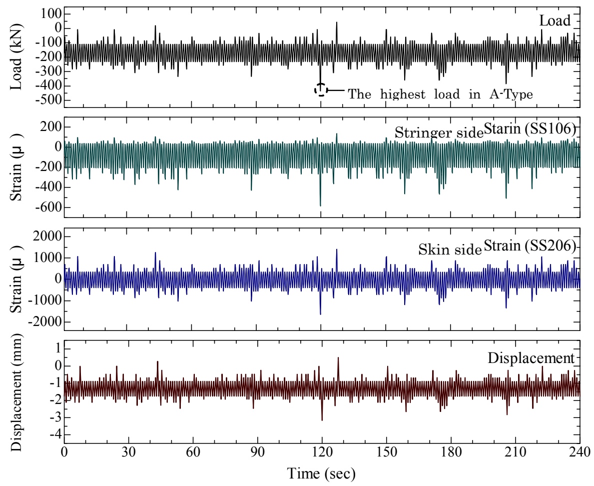

Figure 12.18 Examples of measured data of an A-type flight.

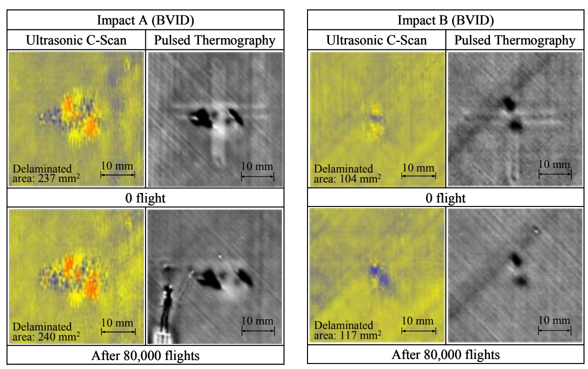

Figure 12.19 Comparison of delamination shapes in BVIDs.

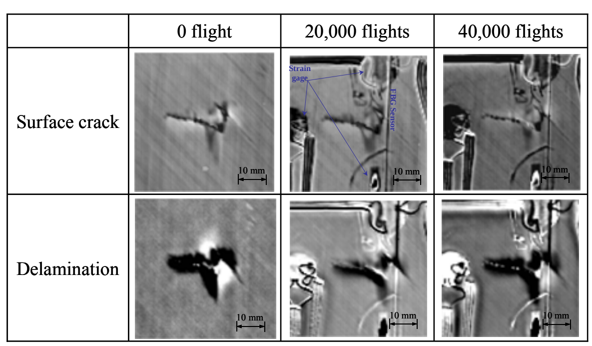

Figure 12.20 Inspection of damage growth using pulsed thermography.

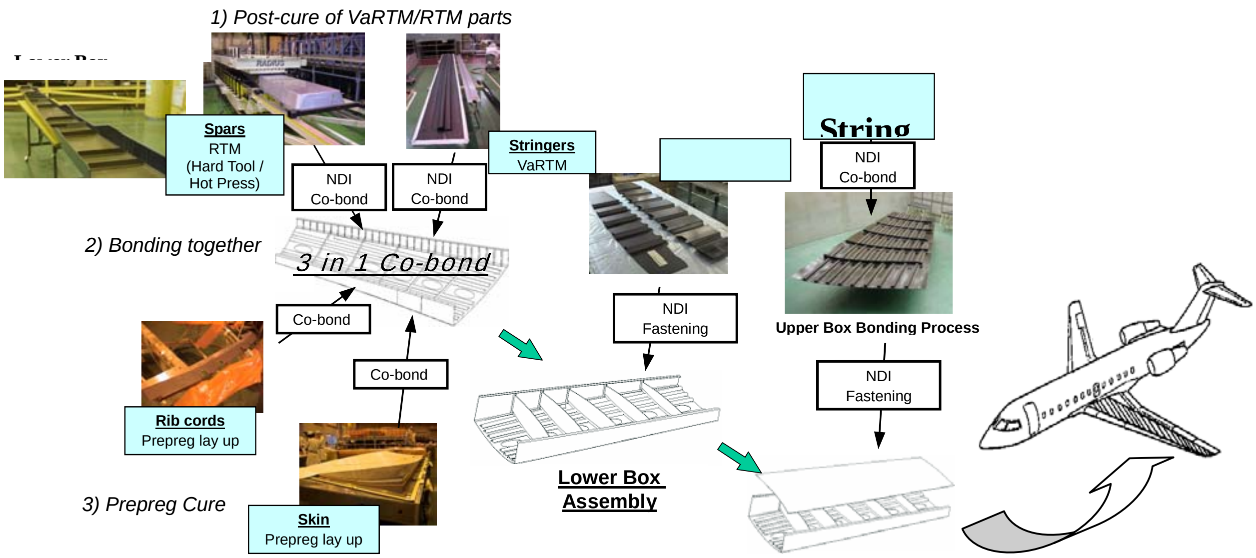

Figure 12.21. Co-bond and assemble process

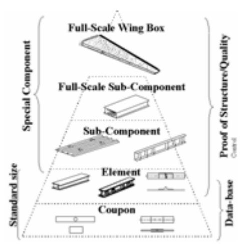

Figure 12.22 Full-scale fabrication try

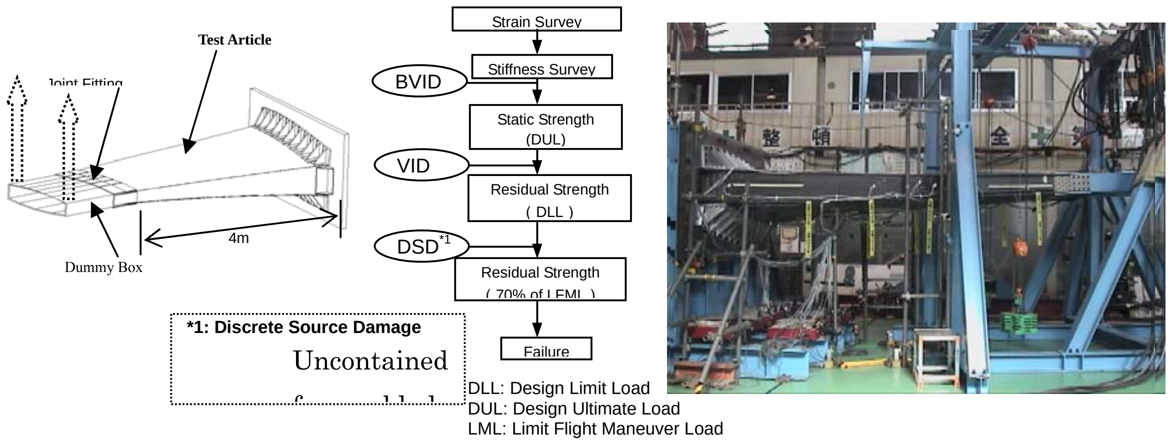

Figure 12.23 Full-scale test fixture and sequence

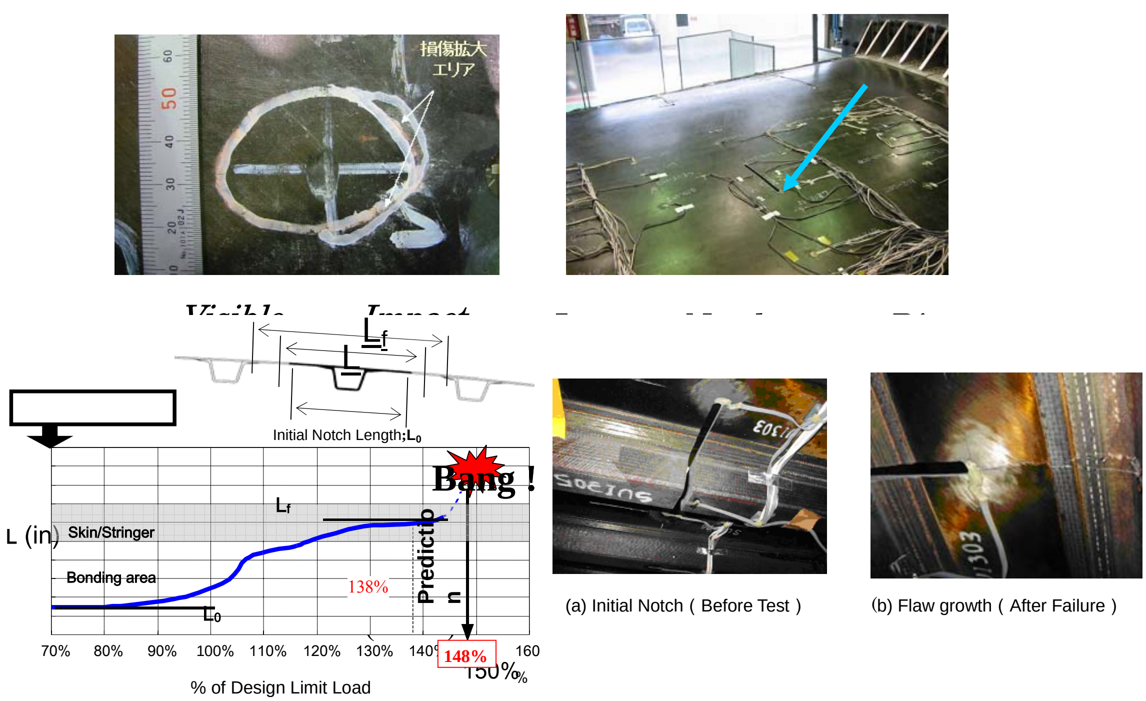

Figure 12.24 Test results and prediction of failure load

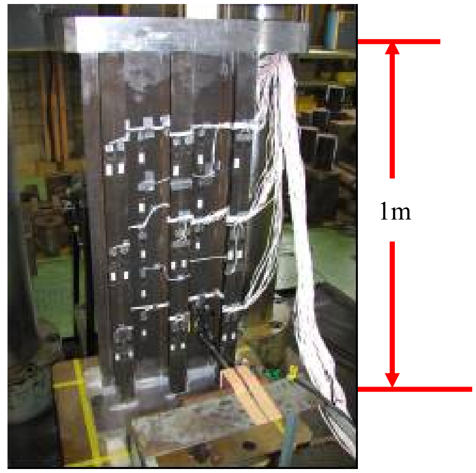

Figure 12.25. 3-stringer co-bonded panel compression test

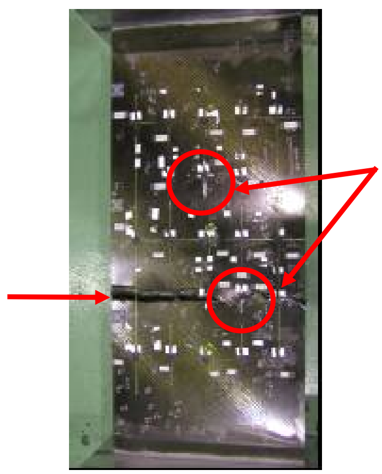

Figure 12.26. Compression test – failure location

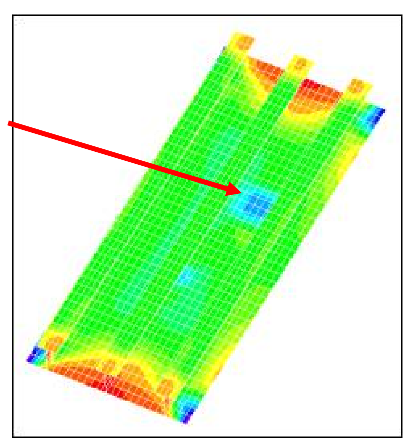

Figure 12.27. Analysis correlation

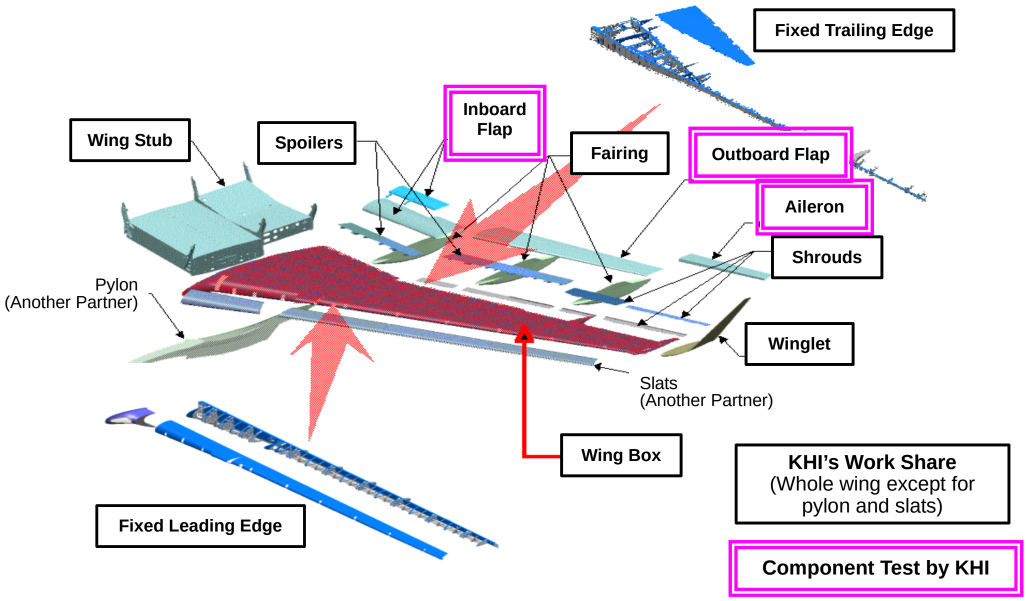

Figure 12.28 Work Share and Component Test Items - EMB190

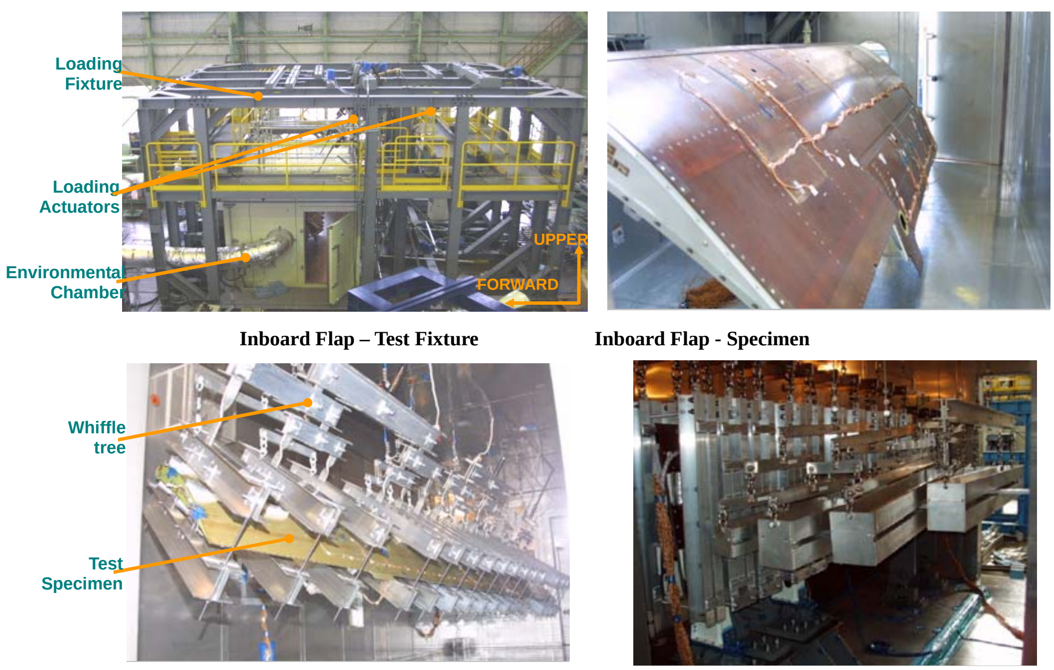

Inboard Flap – Test Fixture

Inboard Flap - Specimen

Outboard Flap - Set up

Aileron - Set up

Figure 12.29 Photographs of full scale component tests - EMB190

(a) Wing root fitting

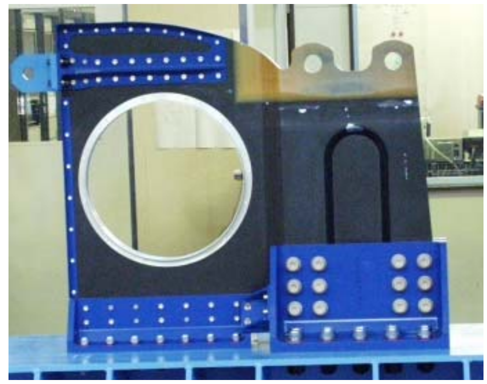

(b) Fuselage carry-through fitting

(c) Horn fitting

(d) Actuator rod and cylinder

Figure 12.30 3-D woven composite fittings

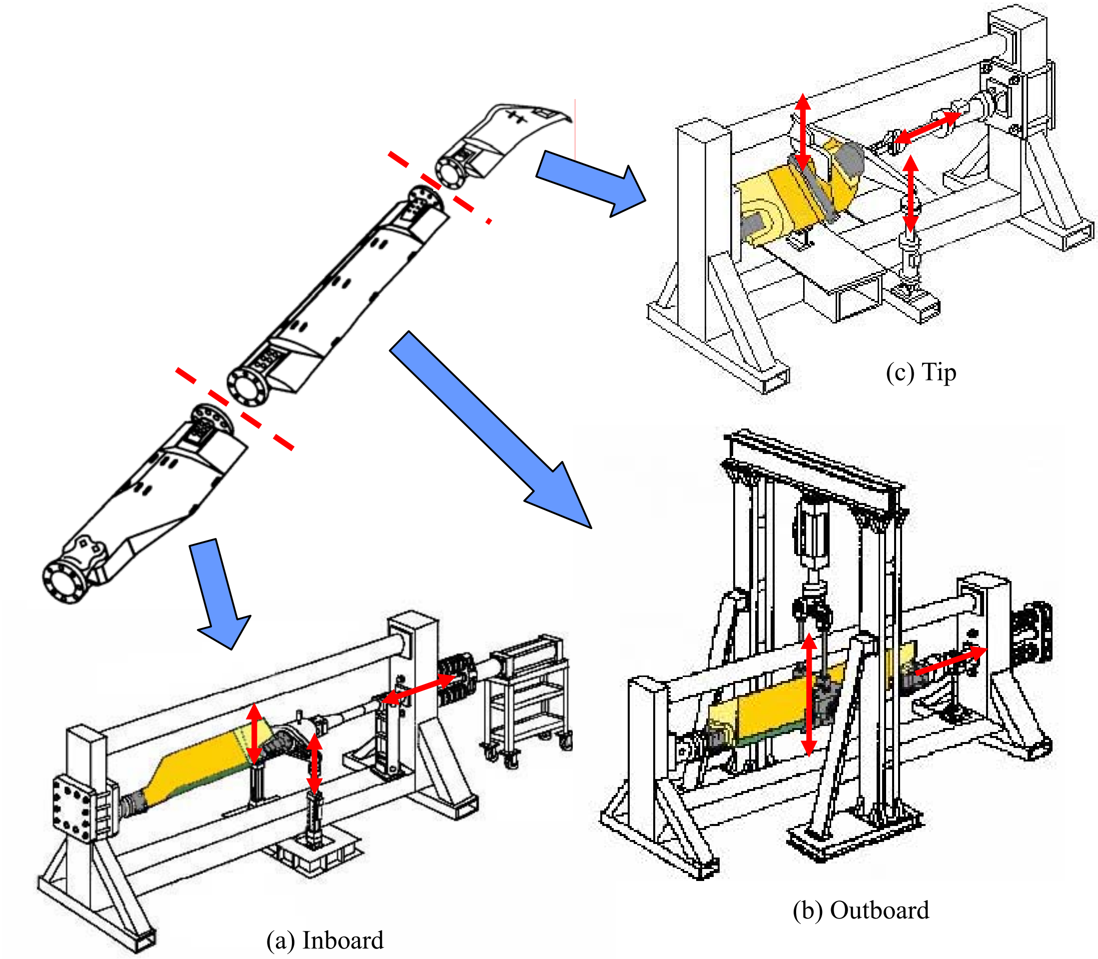

Figure 12.31 Test specimens and instruments of SH-60J KAI MRB fatigue tests

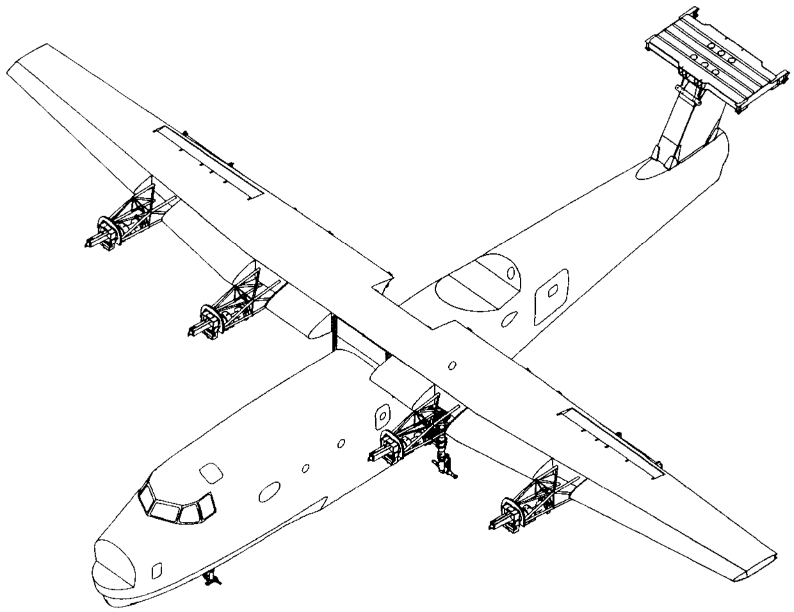

Figure 12.32 Fatigue test article of US-1A KAI

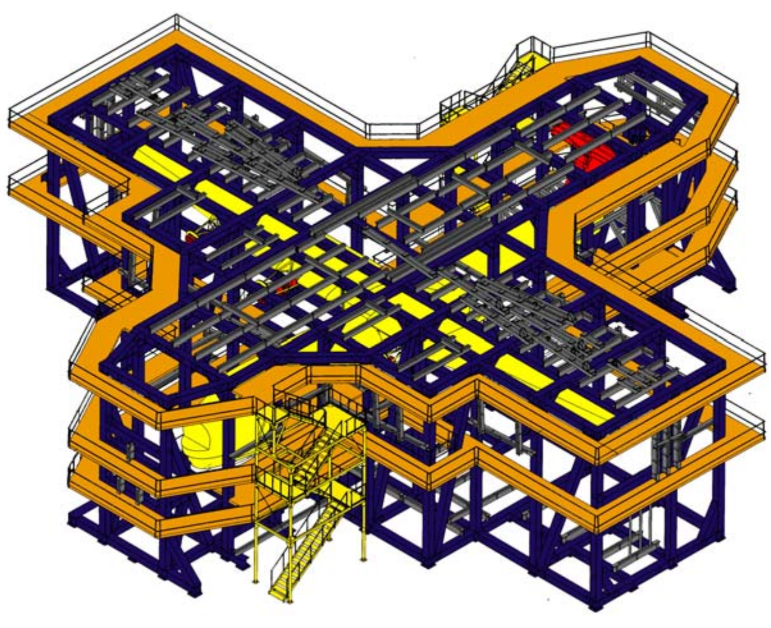

Figure 12.33 Schematic of US-1A KAI FSFT test rig

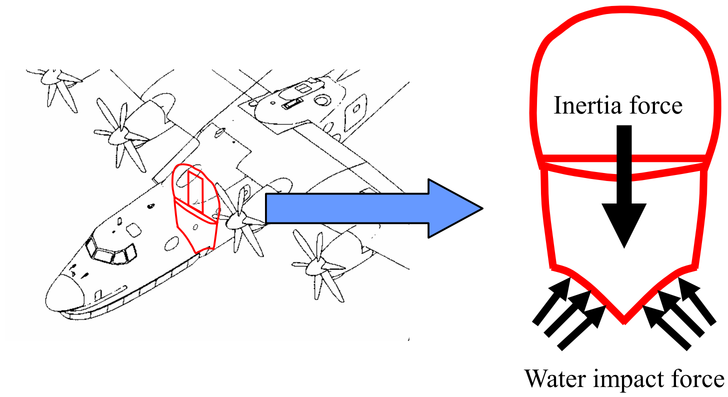

Figure 12.34 Schematic of water loading

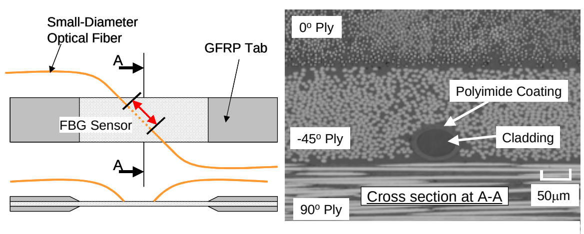

Figure 12.35: A small-diameter FBG sensor embedded in the –45° ply for detection of transverse cracks in the adjacent 90° ply of quasi-isotropic $[45/0/-45/90]_s$ laminate.

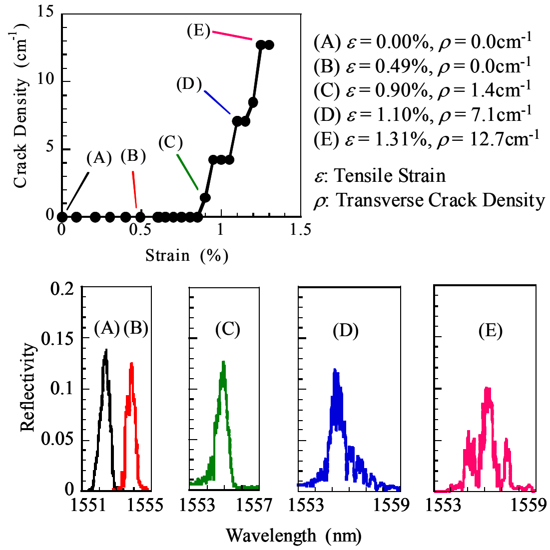

Figure 12.36 Change in wavelength distribution of reflected light from the FBG sensor due to the evolution of transverse cracks.

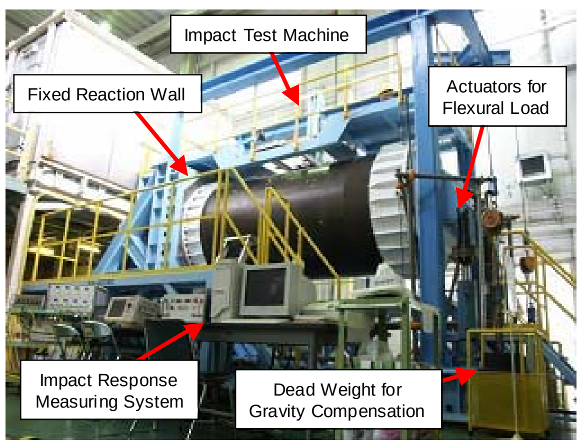

Figure 12.37 Final assembly of the damage detection and suppression demonstrator

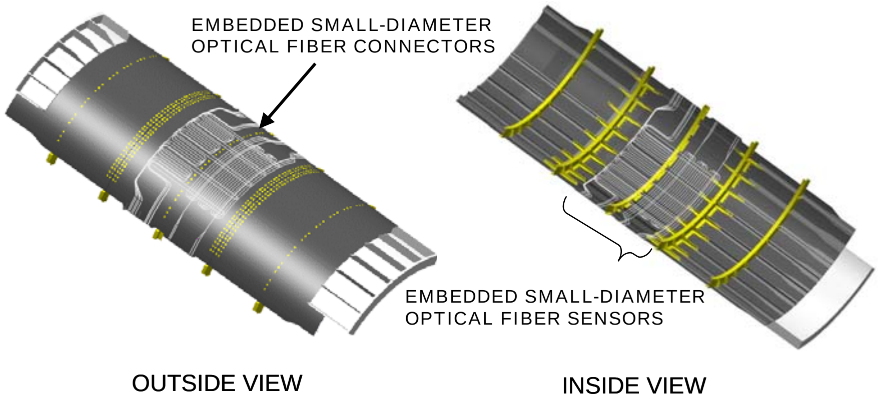

Figure 12.38 Schematic of arrangement of embedded small-diameter optical fibers in the upper panel